Early fatigue damage accumulation of CFRP Cross-Ply laminates considering size and stress level effects

Li, Xi; Benedictus, Rinze; Zarouchas, Dimitrios

DOI
10.1016/j.ijfatigue.2022.106811

Publication date
2022

Document Version
Final published version

Published in
International Journal of Fatigue

International Journal of Fatigue 159 (2022) 106811

Contents lists available at ScienceDirect

International Journal of Fatigue

journal homepage: www.elsevier.com/locate/ijfatigue

Early fatigue damage accumulation of CFRP Cross-Ply laminates considering size and stress level effects

Xi Li *, Rinze Benedictus, Dimitrios Zarouchas

Structural Integrity & Composites Group, Faculty of Aerospace Engineering, Delft University of Technology, Kluyverweg 1, 2629HS, Netherlands

ARTICLE INFO

Keywords:
Acoustic emission
Delamination
Poisson's ratio
Transverse cracking
Stiffness degradation

ABSTRACT

Ply-block size and stress level effect on accumulation of transverse cracks and delamination are investigated during early fatigue life of CFRP laminates. Tension-tension fatigue tests under different stress levels were performed for two cross-ply configurations. Edge observation with digital cameras, digital image correlation and acoustic emission were employed for in-situ damage monitoring. Transverse cracks were dominant for $[0/90_2]_s$ laminates with almost non-existent delamination, while different interactive levels between both damage mechanisms occurred for $[0_2/90_4]_s$ laminates. Poisson's ratio identifies whether early fatigue damage is dominant by transverse cracks or involves delamination. Cumulative AE energy is a helpful indicator of crack density.

1. Introduction

Fatigue damage of composite laminates has attracted considerable attention from research community and industry, in view that laminated structures are inevitable to suffer from fatigue loading during their service life [1]. It is rather complicated to understand and explain, what governs the initiation, accumulation, interaction (synergy or competition) of different damage mechanisms [2]. Intrinsic and extrinsic scatter sources are hard to eliminate during the fatigue testing of laminates, which produce significant dispersion of laboratory data and further hinder our understanding about the progressive accumulation process of fatigue damage [3].

Among mechanical, thermal, acoustic, and optical properties of composites which may be affected by the fatigue damage [4–6], stiffness becomes one of preferable indicators to reflect damage severity. It is relatively easy to measure, and it has been well-correlated to the damage accumulation in a variety of load cases [7–10]. Stiffness usually experiences a three-stage degradation in a rapid-slow-rapid way for composites under fatigue loading [11,12]. Shokrieh and Taheri-Behrooz [13,14] proposed a progressive fatigue damage model to represent this degrading trend of stiffness by assuming that stress redistribution is dominated by off-axis plies and on-axis plies controls the failure of the laminate. As the first stage (Stage I) shows most of the stiffness reduction before the final failure within a short duration period, the corresponding damage process accumulated during this early fatigue life should be significant, thus is worthy to investigate in depth.

Considering that the three-stage stiffness degradation is profound for cross-ply configurations, some progress has been made in our previous work to explore the early fatigue damage accumulation of CFRP $[0_2/90_4]_s$ laminates [15,16]. We achieved in-situ monitoring of transverse matrix cracks and delamination in a relatively large gauge region (~80 mm length), and investigated the initiation, saturation, and interaction of both damage mechanisms. The cross-ply laminates contain a thick 90 block (1 mm nominal thickness − 8 plies of 0.125 mm), because it is easier for the edge observation in a large gauge region. Furthermore, a medium stress level (70% of UTS) was applied during the testing that guaranteed the early fatigue damage would develop in a trackable and measurable way. However, whether the experimental findings from this specific case can represent other cross-ply configurations and stress levels is not clear yet. Therefore, the aim of present work is to expand the knowledge about the early fatigue damage accumulation process of cross-ply laminates considering different ply-block thicknesses and stress levels.

The effect of ply thicknesses or ply-block sizes on the mechanical properties and damage accumulation of laminates is summarised from literature. From thick-ply to thin-ply, laminate quality is improved with the suppression of manufacturing defects [17], while in-situ strength of cracking plies increases significantly [18]. As a result, transverse cracking is delayed, and it may not be able to propagate along the entire width of specimens [19]. Hosoi and Kawada [20] observed that fatigue life of transverse crack initiation is 30 times longer for $[0_2/90_6]_s$ laminates than that of $[0_2/90_{12}]_s$ laminates when the same stress level is

* Corresponding author.
E-mail address: Xi.Li@tudelft.nl (X. Li).

https://doi.org/10.1016/j.ijfatigue.2022.106811
Received 18 November 2021; Received in revised form 21 January 2022; Accepted 16 February 2022
Available online 18 February 2022

imposed on laminates. Kötter *et al.* [21] found that laminates tend to show brittle failure with few visible delamination when ply thickness decreases to a certain threshold. Overall, thin plies or thin ply-blocks inhibit the initiation of both transverse cracks and delamination, enhancing the fatigue life of laminates.

Regarding the stress level effect, Shen *et al.* [22] compared the damage states of $[0/90_4]_s$ specimens with the same transverse crack density, and found that more local delamination appears in the specimens under the lower stress level. Samareh-Mousavi and Taheri-Behrooz [23] found that the fatigue damage governs the development of fatigue mean strain under high stress level while time-dependent viscoelastic strain mainly controls the fatigue mean strain under low stress level. However, Hosoi *et al.* [24] concluded that the change of fatigue damage behaviour, affected by the applied stress levels, was due to the differences of the growth rates of transverse cracks and delamination. The fatigue damage accumulation of laminates under very low stress level is less studied considering the expensive time cost and significant challenges for the analysis of very high cycle and gigacycle fatigue, as reviewed by Shabani *et al.* [25]. Hoang *et al.* [26] proposed linear "*iso*-damage curves" in the semi-logarithmic plane, which describe the fatigue life for laminates to reach a constant crack density at an arbitrary stress level.

It is apparent that the above-mentioned exercises increased our understanding about how the different ply-block/ply sizes and stress levels affect the accumulation of matrix cracks and delamination. However, some aspects focusing on the early fatigue damage accumulation need to be further explored with the help of in-situ damage monitoring techniques [27]. When considering different ply-block sizes and stress levels, it is not clear whether only matrix cracks or both matrix cracks and delamination would be dominant during the early fatigue life. If the accumulation of both damage mechanisms is significant, then the interaction between matrix cracks and delamination should be considered for the analysis of ply-block size and stress level effect, which has not been studied yet so far. Besides, it is also meaningful to investigate how the evolution of mechanical properties (stiffness and Poisson's ratio) and damage-related parameters from in-situ damage monitoring techniques reflect the early fatigue damage accumulation process, which may vary with ply-block sizes and stress levels.

Based on the research aim about investigating the ply-block size and stress level effect on the early fatigue damage accumulation, tension–tension fatigue tests for carbon/epoxy laminates with two different cross-ply laminates were carried out in the present work. Three to four types of maximum cyclic stresses were applied on each ply configuration. During testing, edge observation using digital cameras, digital image correlation (DIC), and acoustic emission (AE) techniques were employed to in-situ monitor the damage accumulation process, i.e., the formation of transverse cracks and the growth of delamination. Afterwards, both the degradation of mechanical properties and the accumulation of different damage mechanisms were characterised.

2. Experimental methods

In this section, the material and manufacturing process of the cross-ply specimens, the cyclic load conditions, and the in-situ damage monitoring system are introduced in detail.

2.1. Material and specimens

Both $[0_2/90_4]_s$ and $[0/90_2]_s$ ply configurations were used in the present work. Unidirectional Prepreg, named Hexply® F6376C-HTS(12 K)-5–35%, was cut and laminated to panels in 300 × 300 mm size. This material contains high tenacity carbon fibres (Tenax®-E-HTS45) and tough epoxy matrix (Hexply® 6376). The nominal ply thickness is 0.125 mm, and fibre volume content is 58%. Laminated panels were then cured inside an autoclave according to recommendation from Hexcel [28]. After curing, these panels were cut to specimens with 250 × 25 mm size based on ASTM D3479/D3479M-19 standard [29]. Thick paper tabs were glued on both ends of the specimen using cyanoacrylate adhesive. Fig. 1(a) shows the geometries and clamping area of designed specimens. The material properties of the UD-Prepreg layer in the cured condition can be found in Table 1 [15]. According to the Classical Lamination Theory, the longitudinal stiffness of $[0_2/90_4]_s$ and $[0/90_2]_s$ laminates is the same, due to the same ratio of the 0-ply thickness to the 90-ply thickness.

2.2. Load conditions

A 60 kN hydraulic fatigue machine was used to perform tension–tension fatigue tests at room temperature. A cyclic loading, with the sinusoidal wave under load control mode, was applied on the clamped specimens. The stress ratio and frequency were fixed at 0.1 and 5 Hz, respectively. The values of maximum cyclic stresses and the corresponding percentage of ultimate tensile strength (UTS) for the two types of ply configurations are listed in Table 2. The UTS was measured by performing ten quasi-static tests, five for each laminate configuration, with 1 mm/min displacement rate, and it was found that the mean value is 723.8 MPa with a standard deviation 9.15 MPa and 800 MPa with a standard deviation 9 MPa for the $[0_2/90_4]_s$ and $[0/90_2]_s$ laminates, respectively. Although sharing the same initial stiffness, UTS is slightly higher for the thinner ply configuration. Therefore, it might not be proper to compare both ply configurations under the stress level which has the same percentage of UTS. Furthermore, the stress of laminates when the first transverse crack occurred, denoted as σ_{90_i}, was also recorded during the quasi-static tests. The detection of the first transverse crack was achieved by capturing images from the edge view every 50 ms using the same in-situ damage monitoring system as it is described in Section 2.3 for the fatigue tests. It was found to be 509.94 MPa and 626.43 MPa for the $[0_2/90_4]_s$ and $[0/90_2]_s$ laminates, accordingly. Then, the maximum cyclic stress divided by σ_{90_i}, also named as the percentage of σ_{90_i} for each stress level, can be obtained, as listed in Table 2. It reflects how severe the applied stress is on the 90 plies, rather than the whole laminate. If the percentage of σ_{90_i} is more than one, then the first transverse crack initiates at the very first cycle; otherwise, the transverse crack initiation delays [30]. Therefore, it would also be interesting to compare both laminates under the stress level which has the similar percentage of σ_{90_i}.

Two to seven tests were repeated for each stress level. After every 500 cycles, a tensile unloading-loading ramp was performed in two seconds, while cameras were taking images at a certain rate (10 or 20 frame-per-second), as shown in Fig. 1(b). For $[0_2/90_4]_s$ laminates, tests executed until the stiffness degradation went through the first stage and it approached the stable phase of the second stage. As for the $[0/90_2]_s$ laminates, tests stopped when the accumulation of transverse cracks reached a saturated state.

2.3. In-situ damage monitoring system

In the present work, a synergistic data acquisition system was built for edge observation, DIC and AE systems, and they were all synchronised with the fatigue machine during testing, as shown in Fig. 1 (c).

Two 9 Megapixel cameras with 50 mm lens were placed at left and right side of the clamped specimen in order to capture the damage accumulation at 90 plies and at 0/90 interfaces; the cameras were monitoring approximately 80 mm of the specimen's length. A thin white paint was applied to the edges so as to create a significant contrast between cracked and uncracked region. After testing, a user-defined image processing algorithm as described in [31] was used to count the number of transverse cracks and measure the length of interlaminar cracks (delamination from the edge view).

Furthermore, a pair of 5 Megapixel cameras with 23 mm lens was installed in front of the specimens for full-field deformation

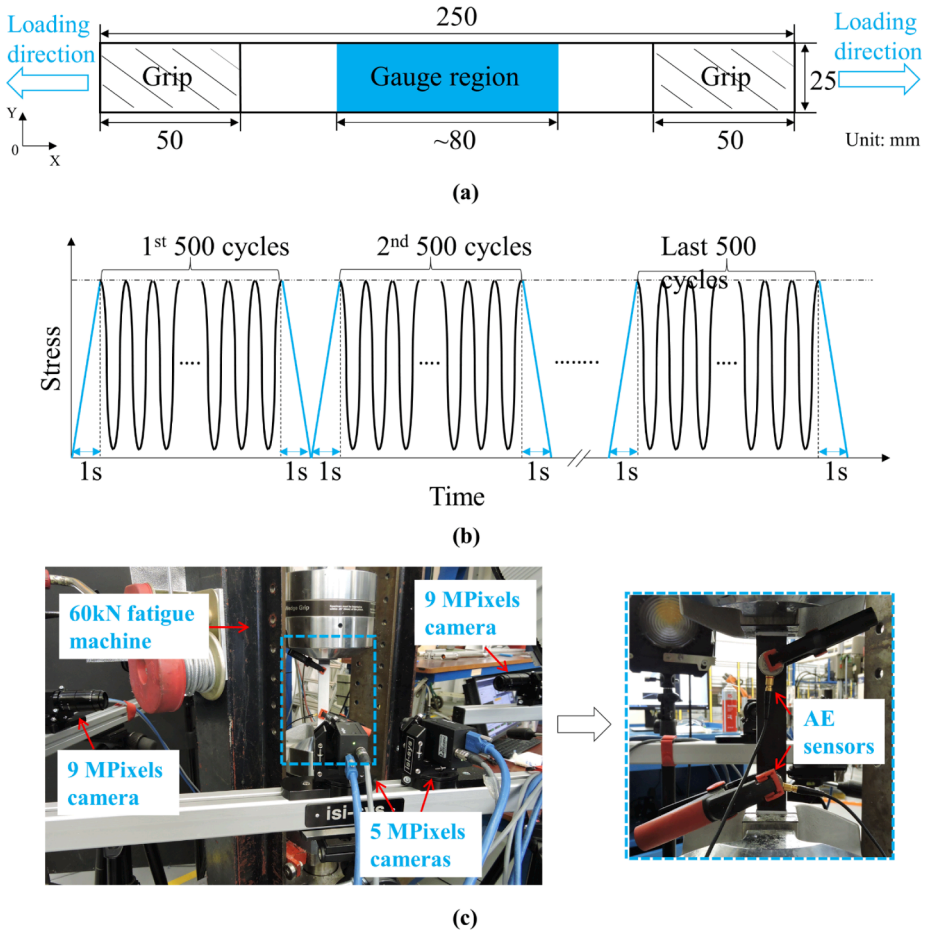

Fig. 1. Specimen dimensions, gauge region and clamping area (a), Loading profile (b) and test set-ups (c) of fatigue tests.

Table 1
Material properties of the unidirectional lamina [15]. ($_T$ - tension; $_C$ - compression).

Material properties	Values
Longitudinal modulus	$E_{11T} = 142$ GPa
Transverse modulus	$E_{22T} = E_{33T} = 9.1$ GPa
In-plane shear modulus	$G_{12} = G_{13} = 5.2$ GPa
Transverse shear modulus	$G_{23} = 3.5$ GPa
Longitudinal strength	$X_T = 2274$ MPa, $X_C = 1849$ MPa
Transverse strength	$Y_T = 102$ MPa, $Y_C = 255$ MPa
In-plane shear strength	$S_{12} = S_{13} = 63$ MPa
Transverse shear strength	$S_{23} = 35$ MPa
In-plane Poisson ratio	$\nu_{12} = \nu_{13} = 0.27$
Transverse Poisson ratio	$\nu_{23} = 0.30$

Table 2
Maximum cyclic stress levels and number of specimens for the fatigue tests. (UTS - ultimate tensile strength; σ_{90_i} - the stress of the first crack initiation).

Stacking sequence	$[0_2/90_4]_s$				$[0/90_2]_s$		
Maximum cyclic stress (MPa)	533	507	480	453	613	560	507
Percentage of UTS (%)	74	70	66	63	77	70	63
Percentage of σ_{90_i} (%)	105	99	94	89	98	89	81
Number of specimens	3	7	6	4	2	2	2

measurements. The cameras covered an ~ 80 × 25 mm gauge area, as shown in Fig. 1(a). This area was firstly painted with the white base coat, where black dots were later printed using a speckle roller with the dot size of 0.18 mm.

Finally, two broadband VS900-M AE sensors with a 100 mm distance were clamped at the specimen. Silicon grease was applied at the surface of the sensors so as to create a sufficient acoustical coupling. The sensors have a diameter of 20.3 mm and a frequency range of 100–900 kHz. The AMSY-6 Vallen system was employed for measuring AE activities, where the sampling rate and the amplitude threshold were set as 2 MHz and 50 dB, respectively. Two pre-amplifiers with gain of 34 dB and band-pass filter of 20–1200 kHz were used to connect the sensors to the acquisition system.

3. Results

The mechanical properties, and damage accumulation process, in the form of transverse cracks and delamination growth, are quantified and presented for both ply configurations.

3.1. Mechanical properties

3.1.1. Longitudinal stiffness

During fatigue loading, the longitudinal stiffness is obtained by the slope of stress–strain relation for each tensile loading ramp (see Fig. 1 (b)). Here, the strain is the average of axial strain at the gauge region of the exterior 0 ply from DIC. Fig. 2 and Fig. 3 show the degradation of normalised longitudinal stiffness E_N/E_0 as a function of fatigue cycles for both ply configurations, where E_0 is the initial stiffness and E_N is the stiffness at the N^{th} cycle.

A significant scatter was found for the stiffness degradation of the $[0_2/90_4]_s$ laminates as presented in Fig. 2, where specimens can be classified into two groups. The classification is based on two

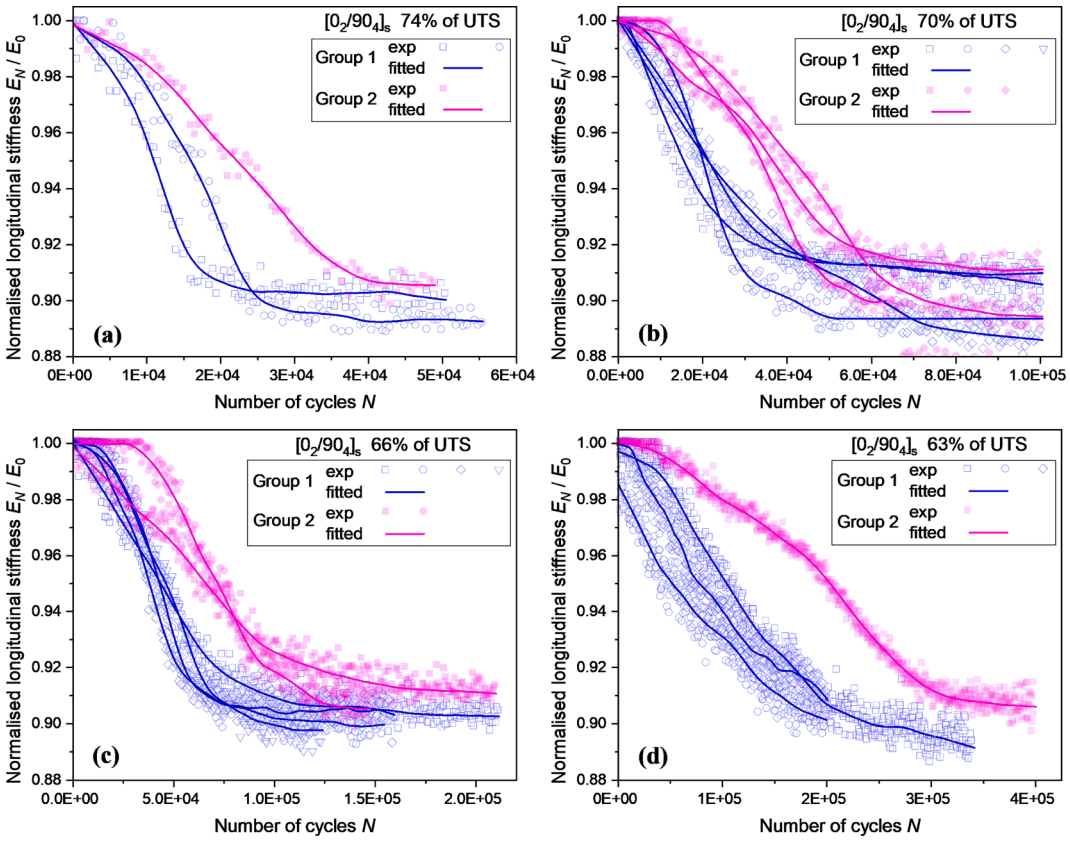

Fig. 2. Normalised longitudinal stiffness versus number of cycles for $[0_2/90_4]_s$ laminates.

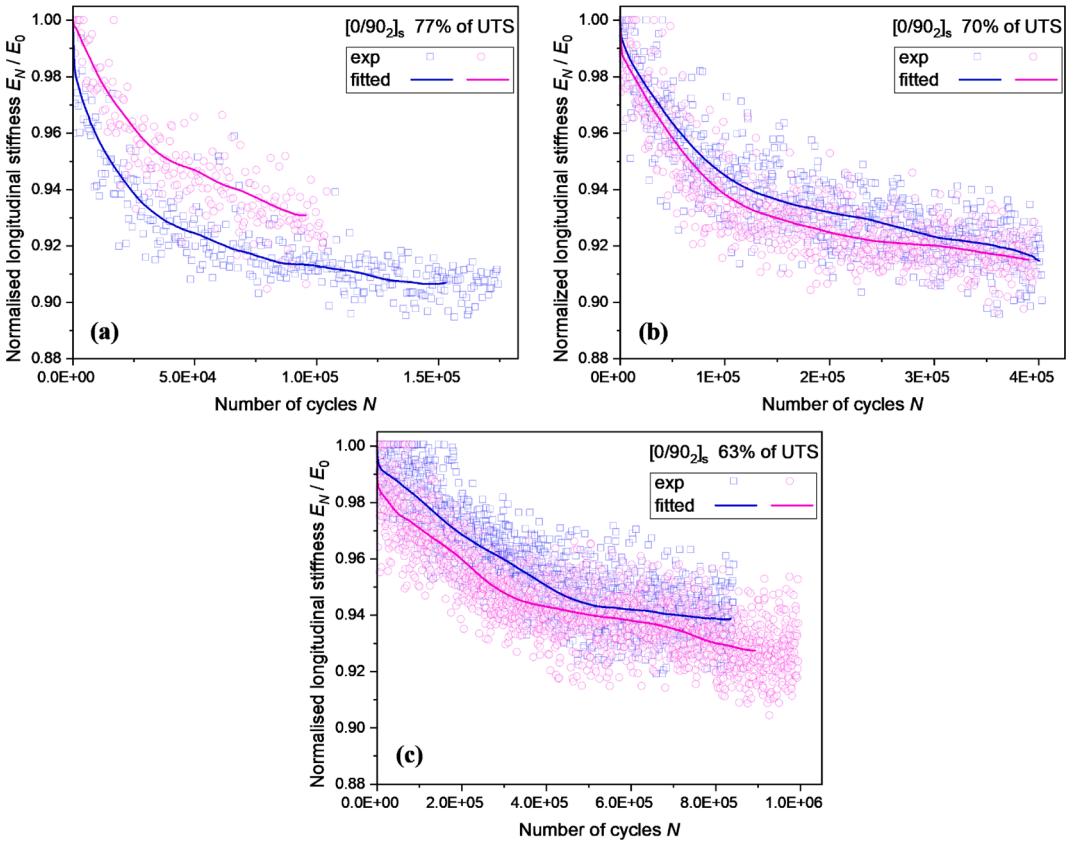

Fig. 3. Normalised longitudinal stiffness versus number of cycles for $[0/90_2]_s$ laminates.

observations: the decreasing rate of E_N/E_0 - N for specimens at Group 1 is about 1.5 to 2.0 times faster than those at Group 2 when the normalised stiffness degrades from 0.98 to 0.92; The Group 2 specimens need significantly more fatigue cycles, e.g. 26% − 74%, to reach the plateau of E_N/E_0 in comparison to Group 1 specimens. The differences about the stiffness degradation between both groups are due to the manufacturing inhomogeneity which produces two levels of fatigue resistance among specimens. This further affects the growth rate of early fatigue damage, as later presented in Section 3.2. As the stress level decreases, the difference of degrading rates between two groups is increasingly significant, which means that the manufacturing inhomogeneity is magnified under low stress level. Until the stiffness reaches the platform, the loss of stiffness in the early fatigue life is about 8–12% of initial stiffness, no matter which stress level is applied.

For $[0/90_2]_s$ laminates, it seems that they experience a bi-linear decrease of stiffness in a rapid-slow manner, as visual in Fig. 3. The stiffness degradation hardly reaches a constant state like $[0_2/90_4]_s$ laminates. Besides, as thin plies restrain the manufacturing defects, the stiffness degradation trends are similar between specimens for a certain stress level. Around 6–10% reduction of stiffness is exhibited in the end of tests, close to the range for $[0_2/90_4]_s$ laminates.

3.1.2. Poisson's ratio

For an example of the $[0_2/90_4]_s$ specimen, Fig. 4 shows that both the axial strain ε_{xx} and transverse strain ε_{yy} vary within the DIC measurement region between two AE sensors. Therefore, to obtain Poisson's ratio ν based on the DIC analysis, the mean value of axial strain $\bar{\varepsilon}_{xx}$ and the mean value of transverse strain $\bar{\varepsilon}_{yy}$ at the gauge region are firstly extracted, and then ν is calculated as $-\frac{\bar{\varepsilon}_{yy}}{\bar{\varepsilon}_{xx}}$.

Fig. 5 and Fig. 6 present the evolution of Poisson's ratio as a function of fatigue cycles for both ply configurations. For most of specimens with thick 90 plies, Poisson's ratio significantly increases as a function of fatigue cycles, as shown in Fig. 5. Our previous work [15] has explained that this phenomenon is due to the increase of absolute transverse strain caused by the Poisson contraction at delaminated region, as also reported by Oz *et al.* [32]. For each group of $[0_2/90_4]_s$ specimens, a scattering evolution of Poisson's ratio is presented under all stress levels. This phenomenon indicates the accumulation of delamination varies among specimens which share a similar trend of stiffness degradation.

Unlike $[0_2/90_4]_s$ laminates, specimens with thin 90 plies show the opposite (see Fig. 6). The absolute values of transverse strains at the 0 plies decrease with the increase of fatigue cycles. In view that this decrease is negligible, transverse strains can be regarded as constant during the fatigue tests. Thus, it is mainly the increase of the axial strain causes the decrease of Poisson's ratio as fatigue cycles increase. It can also be inferred that no significant delamination grew at the interface between 0 and 90 plies for the $[0/90_2]_s$ laminates.

As a result, transverse cracks govern the decrease of Poisson's ratio for the $[0/90_2]_s$ laminates, while the increase of Poisson's ratio for the $[0_2/90_4]_s$ laminates is attributed to delamination. From this point of view, Poisson's ratio could be considered to identify whether the early fatigue damage of a cross-ply laminate is dominant by transverse cracks or involves delamination.

3.2. Damage accumulation process

3.2.1. Transverse cracks

For both ply configurations, most of transverse cracks propagated through the width direction within 500 cycles. As observed by digital cameras, the number of transverse cracks and their location at 90 plies were almost the same for both left and right sides after every 500 cycles. Besides, when a transverse crack forms at inner 90 plies, the axial strain concentration, across the entire width of the laminate, is induced at the related position of the exterior 0 ply. For the examples of both ply configurations tested under 70% of UTS, Fig. 7 presents the distribution of axial strain concentrations within the gauge region at four different

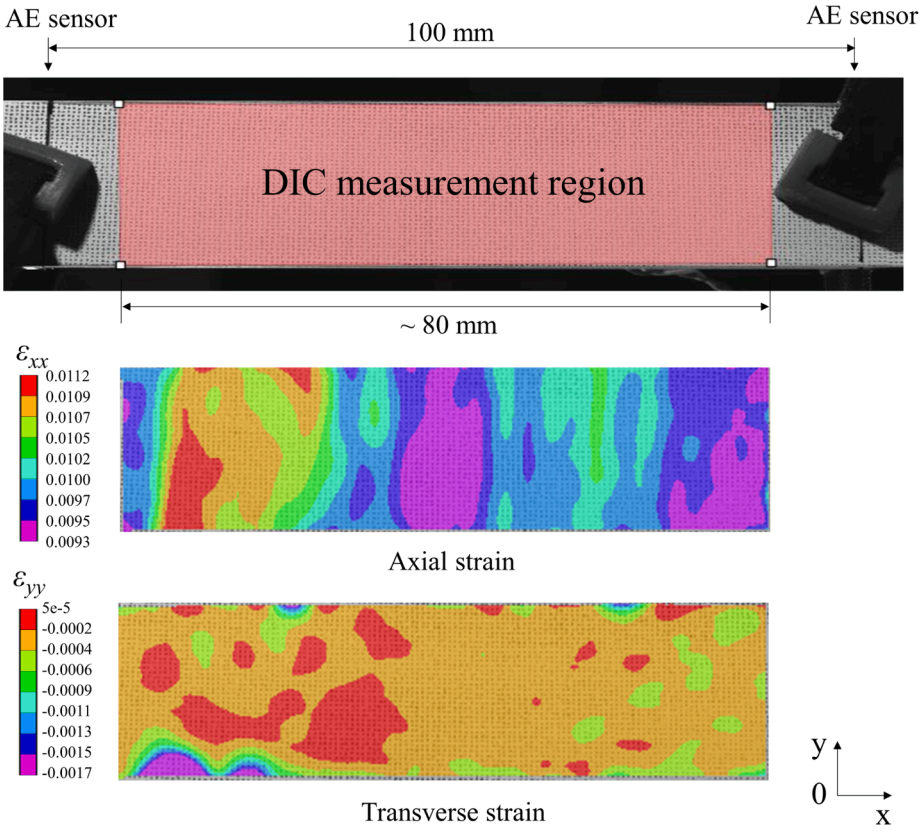

Fig. 4. The axial and transverse strain distribution at the gauge region for one of $[0_2/90_4]_s$ laminates at the 8500th cycle.

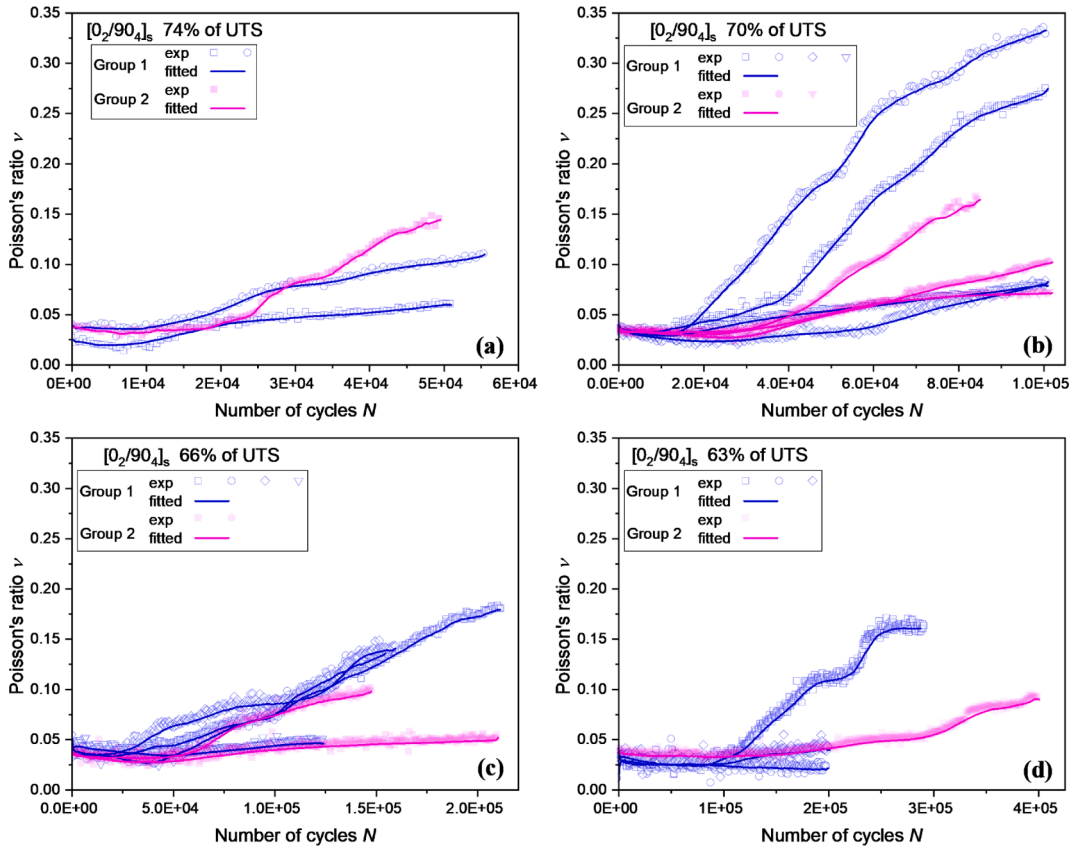

Fig. 5. The change of Poisson's ratio at the exterior 0 ply as a function of number of cycles for $[0_2/90_4]_s$ laminates.

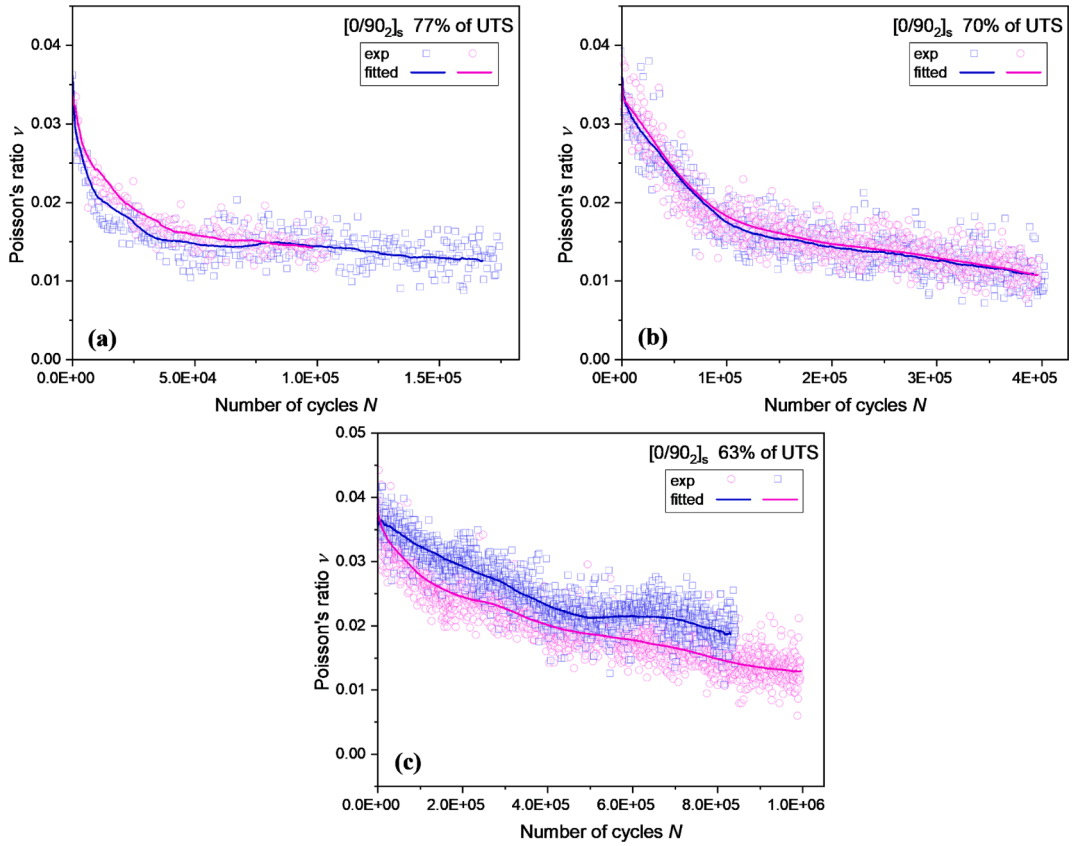

Fig. 6. The change of Poisson's ratio at the exterior 0 ply as a function of number of cycles for $[0/90_2]_s$ laminates.

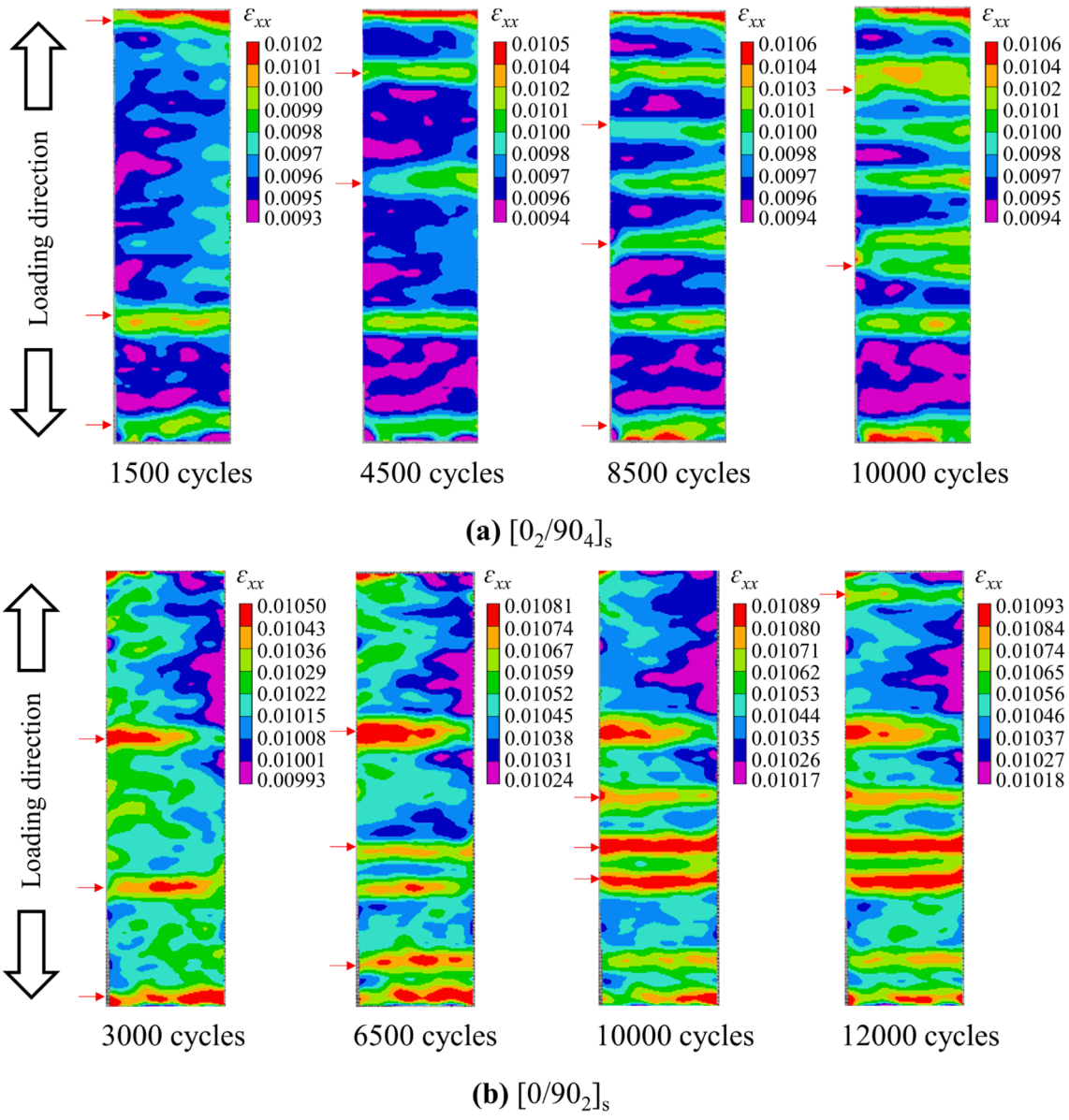

Fig. 7. Evolution of axial strain distribution at the gauge region as fatigue cycles increases for the $[0_2/90_4]_s$ laminate and the $[0/90_2]_s$ laminate.(ε_{xx} - axial strain).

moments. Red arrows mark the location of new cracks generated at certain fatigue cycles.

A good correlation can be observed between the location of new cracks at 90 plies and newly formed concentration of the axial strain at the 0 ply. When the new crack closes to neighbouring cracks, an expansion of the original axial strain concentration can be observed at the related local region; otherwise, an extra axial strain concentration is formed at the gauge region.

The evolution of crack density ρ at 90 plies is obtained as a function of fatigue cycles for both ply configurations, as shown in Fig. 8 and Fig. 9 (see scatter plots). ρ is calculated as the average of number of transverse cracks counted from both left and right sides, which is then divided by the gauge length (~80 mm).

For $[0_2/90_4]_s$ laminates, the evolution of crack density scatters among specimens with a similar stiffness degradation trend. A linear increase of crack density can be observed at the very early fatigue life. Once reaching a certain threshold, which differs among specimens, a gradual decrease of the growth rate is observed, till the occurrence of characteristic damage state (CDS, also known as saturation of transverse cracks). However, transverse cracks saturate at the density ranging from ~ 0.2 to ~ 0.4 mm^{-1} for each group of specimens, regardless of stress levels, as also reported by Pakdel and Mohammadi [33]. In addition, a negative correlation between saturated crack density and fatigue cycles to reach CDS is found for each stress level. Specimens which spend more time to reach CDS have a lower saturated crack density, and vice versa. These similarities indicate that the characteristic damage state is independent of stress levels for $[0_2/90_4]_s$ laminates.

Different from $[0_2/90_4]_s$ laminates, Fig. 9 presents bi-linear growing trends of crack density for $[0/90_2]_s$ laminates. When the crack density reaches around 0.8 mm^{-1}, crack evolution changes from the first linear part to the second one which accompanies with a very slow growing rate. Consequently, a constant crack density is hard to achieve as fatigue cycles increase. Therefore, the saturation of transverse cracks (or CDS) here is defined as the moment when the crack density approaches to 1 mm^{-1}. The saturated crack density is approximately 2–5 times larger than that of $[0_2/90_4]_s$ laminates. Carraro *et al.* [34] and Pakdel and Mohammadi [33] also found that the crack density at the saturated state is higher for cross-ply laminates with thinner 90 plies. As stress relaxation around a transverse crack is narrower for thinner cracking plies [22,35], more high-stress region exists at the cracking plies to support

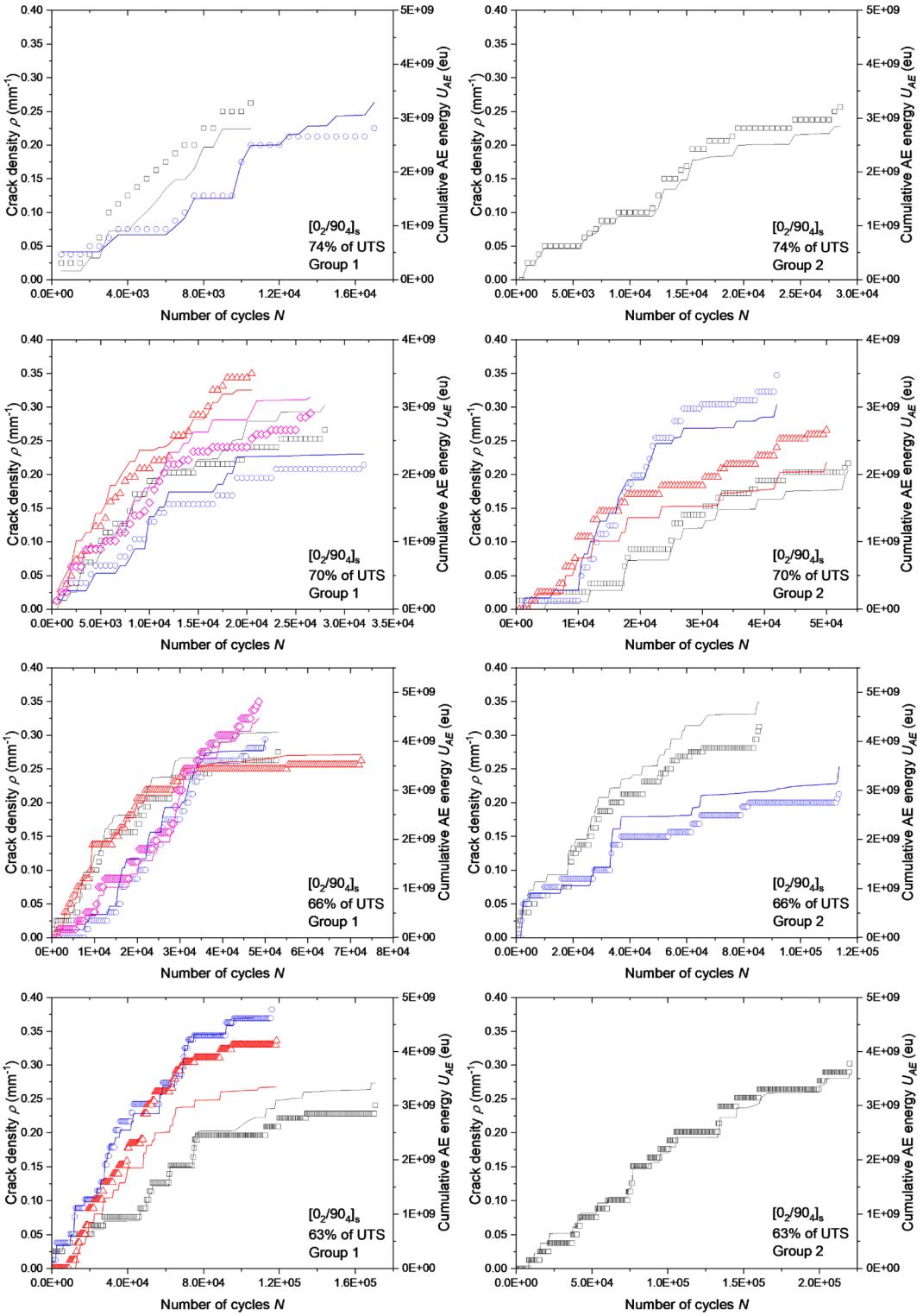

Fig. 8. The evolution of crack density (scatter plots) and cumulative AE energy (line plots) as a function of fatigue cycles for two groups of $[0_2/90_4]_s$ laminates.

the transverse crack initiation. In addition, local delamination is easier to emerge for thicker cracking plies, as the energy release rate to drive the delamination propagation at a transverse crack tip is lower [34]. This fact further widens the region of stress relaxation and restrains the transverse crack initiation at thick plies. Therefore, $[0/90_2]_s$ laminates present higher chances to form transverse cracks with a larger number presented at the saturated state, in comparison with $[0_2/90_4]_s$ laminates.

As AE activity was recorded during the fatigue tests, it would be interesting to explore AE features related to transverse cracks. Literature [36–38] has showed that cumulative AE hits, counts and energy with the increase of number of cycles could signify different stages of damage accumulation under fatigue loading. In view that AE energy has showed the potentials to predict accumulation of transverse cracks under static tensile loading [31,39], the relation between AE energy and crack density is further explored here for fatigue loading. A localisation

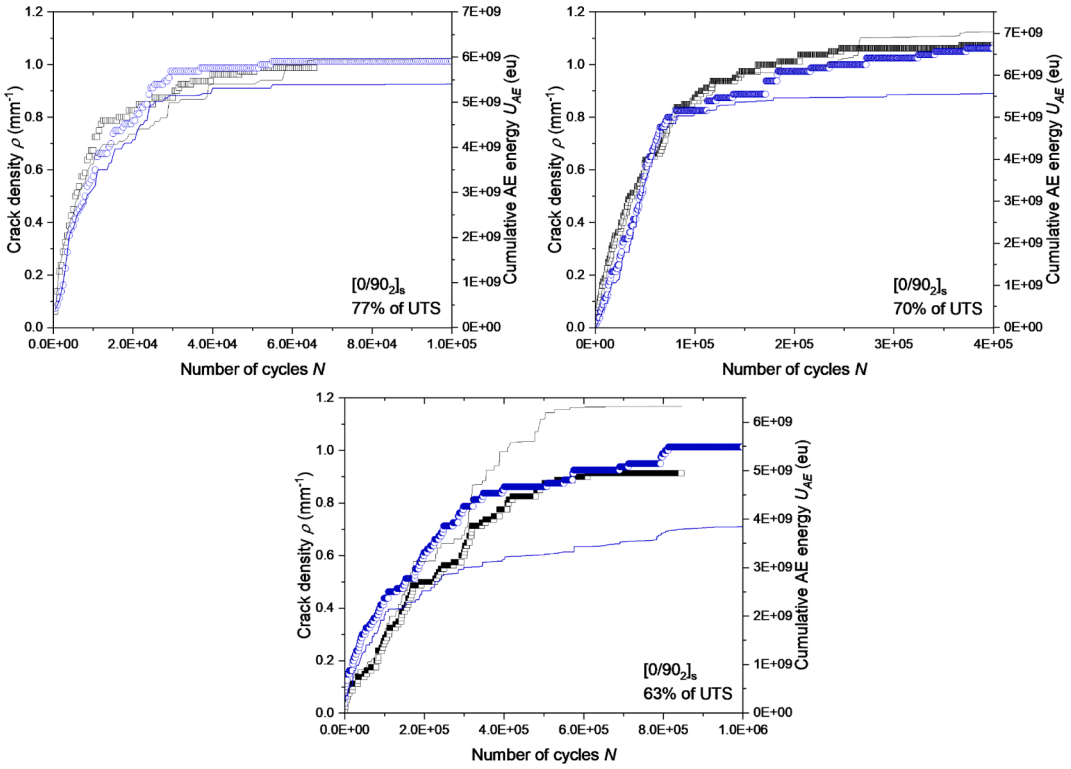

Fig. 9. The evolution of crack density (scatter plots) and cumulative AE energy (line plots) as a function of fatigue cycles for $[0/90_2]_s$ laminates.

algorithm is firstly applied to filter out AE signals which are out of the gauge region. Then, cumulative energy U_{AE} of recorded AE signals is calculated as a function of fatigue cycles, as shown in Fig. 8 and Fig. 9 (see line plots). Here, the AE energy of each signal is defined as the area under the squared signal envelope [27]. As observed, the growing trends of cumulative AE energy are well correlated to those of crack density, especially the sudden jumps. This indicates that transverse cracks are the main damage source to produce AE signals carrying high released energy for two types of cross-ply laminates.

Furthermore, a linear relation between crack density and cumulative AE energy until the saturation of transverse cracks is presented in Fig. 10 and Fig. 11. The slop of U_{AE}-ρ curves for $[0_2/90_4]_s$ laminates is about

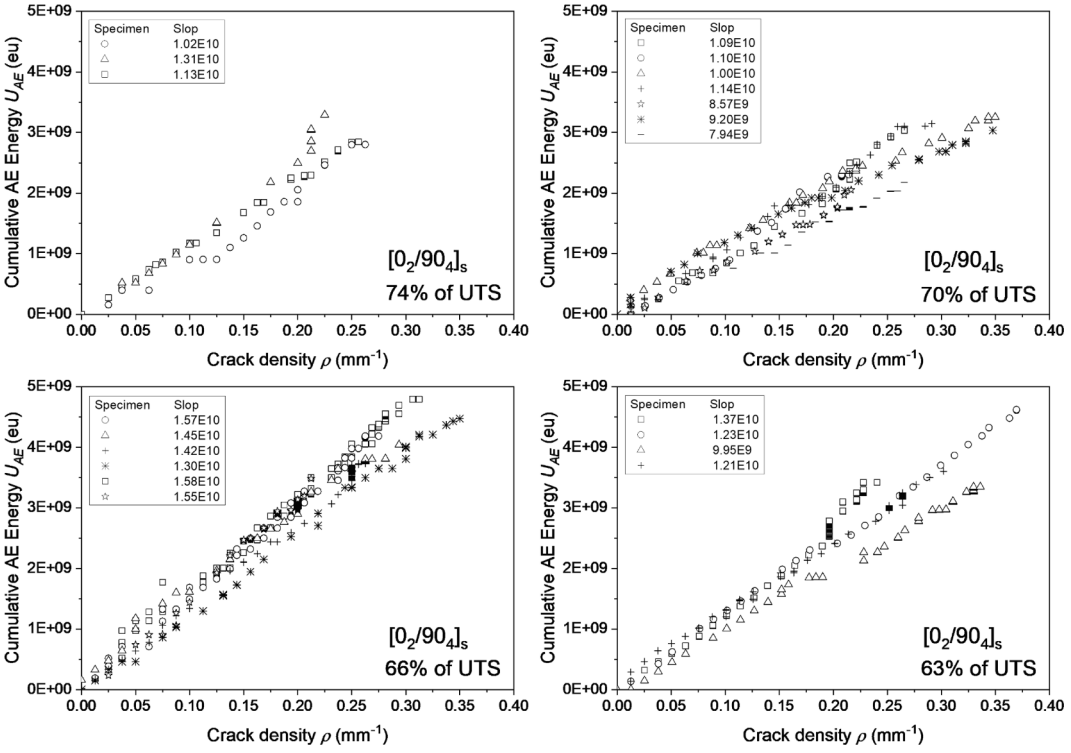

Fig. 10. The linear relation between crack density and cumulative AE energy for $[0_2/90_4]_s$ laminates under different stress levels.

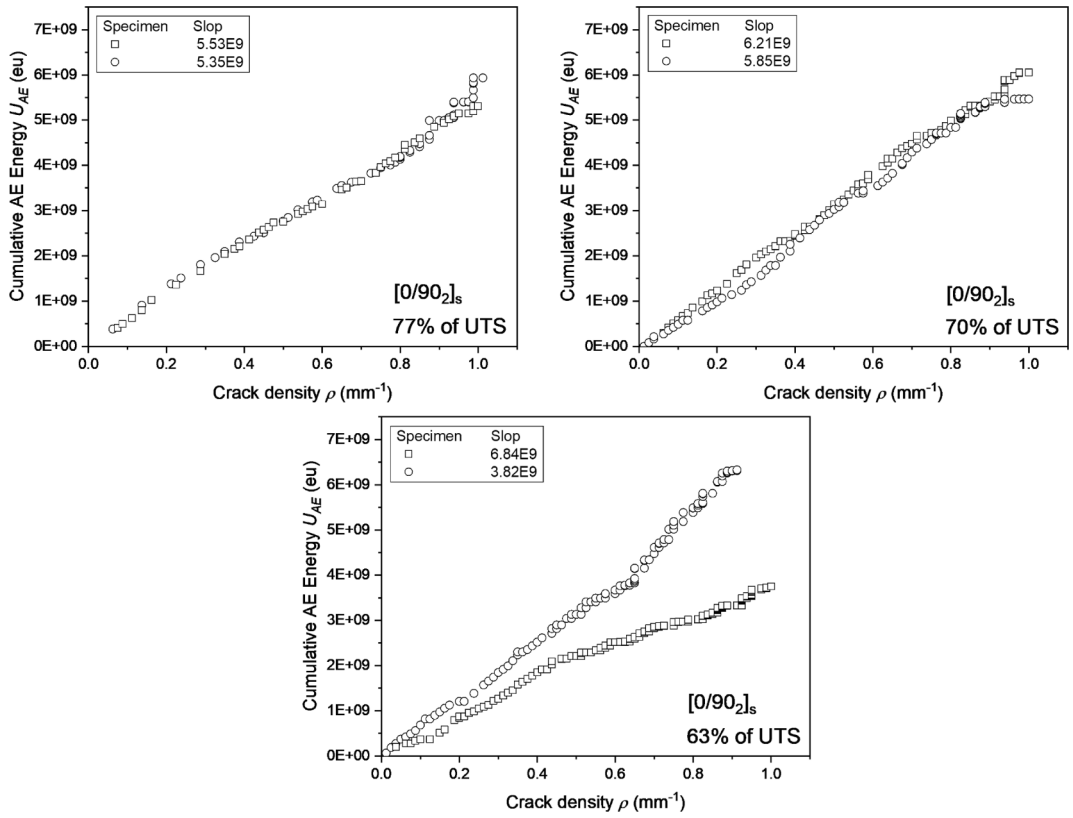

Fig. 11. The linear relation between crack density and cumulative AE energy for $[0/90_2]_s$ laminates under different stress levels.

twice of that for $[0/90_2]_s$ laminates. This phenomenon implies that the released energy from a transverse crack at thick 90 plies is higher than that at thin 90 plies for the same material system, as the crack surface is different for both types of laminates. Overall, cumulative AE energy can be regarded as an indicator of crack density for cross-ply laminates.

3.2.2. Delamination

During the fatigue loading, delamination is significant for most of $[0_2/90_4]_s$ laminates, while almost no delamination is found for $[0/90_2]_s$ laminates as the thin 90 block inhibits the growth of delamination [21]. Because transverse cracks and delamination coexist and complex the accumulation of early fatigue damage, it is necessary to quantify the evolution of delamination for the $[0_2/90_4]_s$ laminates.

From the edge view, we observed that interlaminar cracks initiated from transverse crack tips and propagated at 0/90 interfaces along the length direction. Interlaminar crack ratio, obtained as the ratio of interlaminar crack length to the gauge length, is used to quantify the delamination propagation along edges. Fig. 12(a) plots the evolution of interlaminar crack ratio as a function of fatigue cycles for different stress levels. Considering the quantification of delamination growth towards the width direction, our previous work [15,16] has showed a correlation among Poisson's ratio, area of transverse strain concentration at the exterior 0 ply and delamination area. With the increase of delamination area, more 90 plies are separate from 0 plies. As a result, 0 plies become flexible and perform significant Poisson effect, and transverse strain concentration at the exterior 0 ply is created at delaminated region. Based on these findings, the evolution of normalised delamination area as a function of fatigue cycles can be obtained, as presented in Fig. 12(b). Here, normalised delamination area is the area of transverse strain concentration at the exterior 0 ply divided by the gauge area.

The increase of interlaminar crack ratio experiences a slow-rapid-slow process, while normalised delamination area seems to increase linearly with the applied fatigue cycles. When the stiffness degradation approaches the second stage, the gauge region is almost fully delaminated along edges; however, delamination propagates less than the half of the area of the gauge region for most specimens, as observed in Fig. 12. Besides, most of transverse strain concentrations locate near edges, further indicating that delamination propagated faster along the edges than though the width. Like the accumulation of transverse cracks, delamination propagation during the early fatigue life scatters among each group of specimens, indicating the existence of different levels of interaction between both damage mechanisms for the $[0_2/90_4]_s$ laminates.

4. Discussions

In this section, the effect of ply-block sizes and stress levels on the accumulation of early fatigue damage are further explored based on the degradation of material properties as well as accumulation of transverse cracks and delamination.

4.1. Size effect on early fatigue damage accumulation

During the early fatigue life, both types of cross-ply laminates experience the accumulation and saturation of transverse cracks. The growing trend of crack density initiates from a linear increase followed by a decrease of the growth rate. For $[0_2/90_4]_s$ laminates, the decrease of growth rate is mainly due to the propagation of delamination which restrains the initiation of new cracks. As for $[0/90_2]_s$ laminates, the severe interaction between new and prior cracks could be presented from the moment with a large crack density. This is because higher chances are provided that new cracks will initiate near prior cracks, where the stress of 90 plies is redistributed and it is lower than the applied maximum stress on 90 plies [40,41]. As a result, more fatigue cycles are needed for the initiation of a new crack, thus a decrease of the growth rate is caused after crack density reaches around 0.8 mm^{-1} (see Fig. 9).

As different stress levels were involved during the fatigue tests,

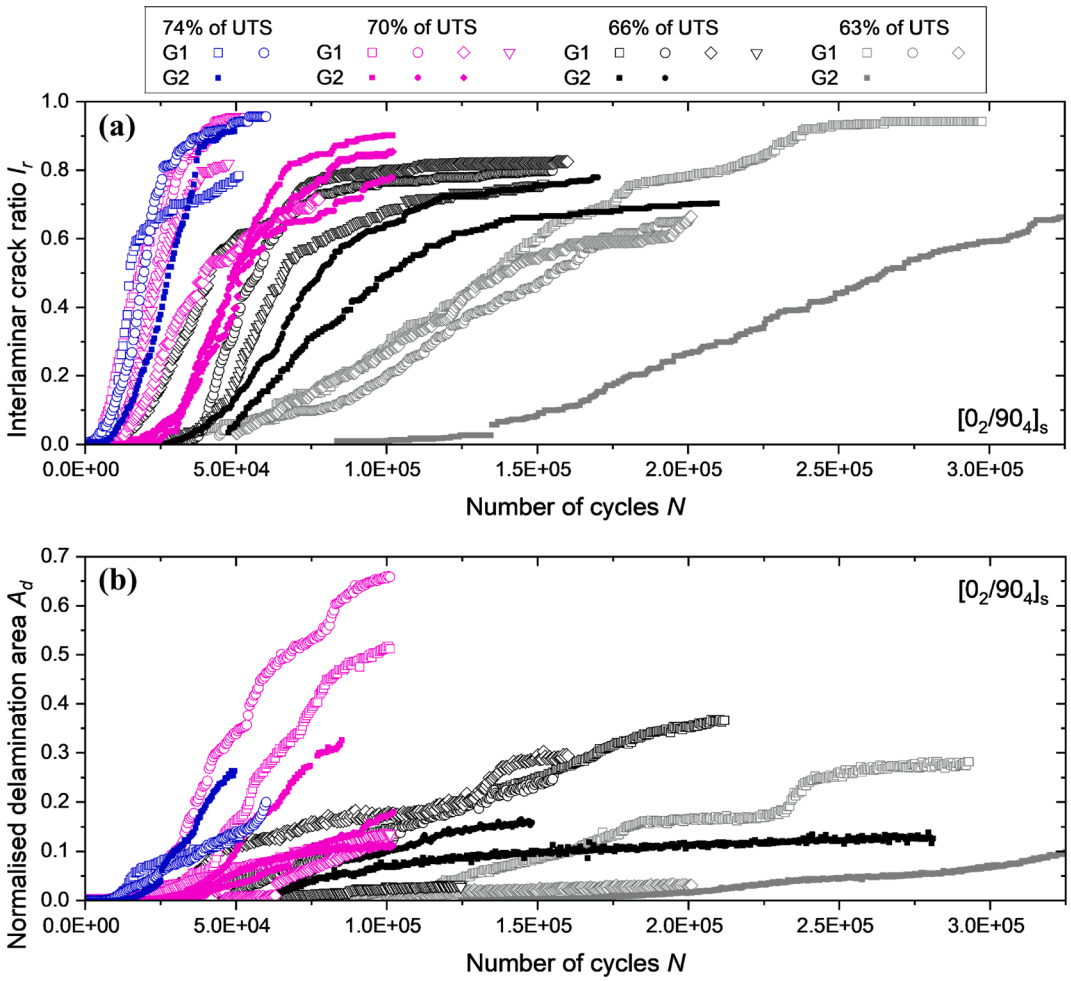

Fig. 12. The evolution of interlaminar crack ratio (a) and normalised delamination area (b) as a function of fatigue cycles. (G1-Group 1; G2-Group 2).

Fig. 13 compares the evolution of crack density as a function of fatigue cycles under the same stress levels. Here, two different ways, as introduced in Section 2.2., are used to calculate the stress level: one refers to the whole laminate and the other refers to the 90 plies. Crack density of each specimen is normalised by its saturated crack density. When the stress level for the whole laminates is the same, a slow accumulation of transverse cracks is presented for $[0/90_2]_s$ laminates (see Fig. 13 (a) and (b)). Besides, the consumed fatigue cycles to reach the saturation of transverse cracks is about five times longer than that of $[0_2/90_4]_s$ laminates. As listed in Table 2, under the stress level at either 70% or 63% of UTS, the corresponding stress level for 90 plies of $[0/90_2]_s$ laminates is 9–10% lower than that of $[0_2/90_4]_s$ laminates, thus increasing their resistance to the initiation of transverse cracks. When the comparison about the evolution of normalised crack density is under a similar stress level for 90 plies, a new insight can be provided to bridge the evolution of transverse cracks for both cross-ply laminates; it is the stress level for 90 plies that mainly controls how fast the saturation of transverse cracks occurs. As presented in Fig. 13 (c) and (d), the growing rate of normalised crack density for $[0/90_2]_s$ laminates is close to that of $[0_2/90_4]_s$ laminates in the Group 1. In particular, the first linear increase of normalised crack density with the increase of fatigue cycles is almost the same for both ply configurations.

As the initial stiffness is the same for both cross-ply laminates, how transverse cracks affect stiffness for each type of laminates is further investigated. Fig. 14 presents the decrease of normalised longitudinal stiffness as crack density increases. For $[0_2/90_4]_s$ laminates, a linear relation between crack density and degraded stiffness is presented at the beginning of crack accumulation. When crack density reaches a certain threshold, which differs from specimen to specimen, the deceasing rate of stiffness suddenly increases and becomes more and more aggressive for the remaining fatigue cycles. This is because another damage mechanism, delamination, starts to play a role in degrading the stiffness. However, for $[0/90_2]_s$ laminates, the degrading trend of stiffness remains linear during the entire process of transverse crack accumulation. This phenomenon further indicates that no significant delamination grew at the 0/90 interfaces during the early fatigue life to degrade stiffness. By fitting the linear parts of plots in Fig. 14, it is observed that the decrease of stiffness caused by transverse cracks shows a slow rate for $[0/90_2]_s$ laminates, which is about half of that for $[0_2/90_4]_s$ laminates. This difference is because that area of a transverse crack surface for $[0/90_2]_s$ laminates is smaller that of $[0_2/90_4]_s$ laminates [42].

4.2. *Stress level effect on early fatigue damage accumulation*

The effect of stress levels on the early fatigue damage accumulation is reflected on the growth rates of damage mechanisms, in accordance with the conclusion from Hosoi *et al.* [24]. The higher the stress level is, the faster the growth rates of crack evolution and delamination propagation present. Except this, early fatigue damage accumulation is similar among different stress levels. As presented in Fig. 14, for both cross-ply laminates, the normalised longitudinal stiffness degraded by transverse cracks shows a similar decreasing trend with the increase of crack density, irrespective of applied stress levels. In particular, the nonlinear decease of E_N/E_0 plotted in Fig. 14(a), due to the coexistence of transverse cracks and delamination, is also similar among specimens with a similar saturated crack density.

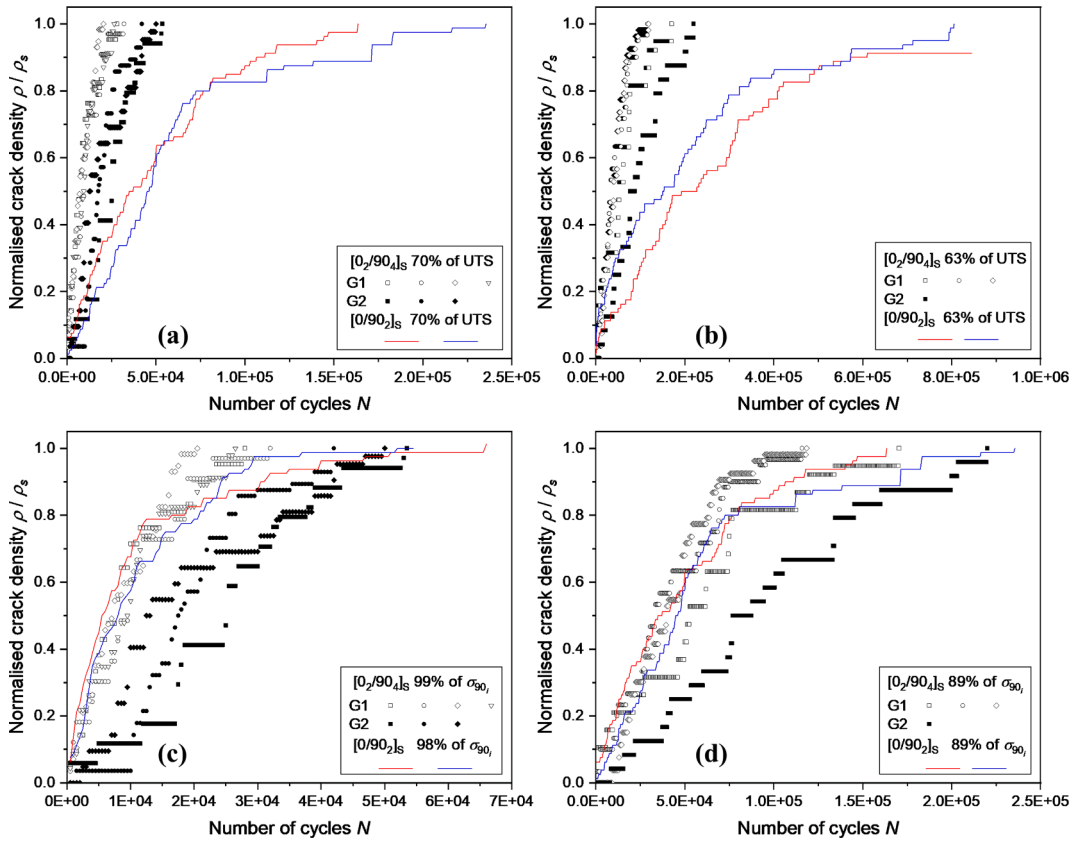

Fig. 13. Comparison about the increase of normalised crack density as a function of fatigue cycles for both ply configurations: (a) stress level at the 70% of UTS; (b) stress level at the 63% of UTS; (c) stress level at 98–99% of σ_{90_i}; (d) stress level at 89% of σ_{90_i}. (G1-Group 1; G2-Group 2).

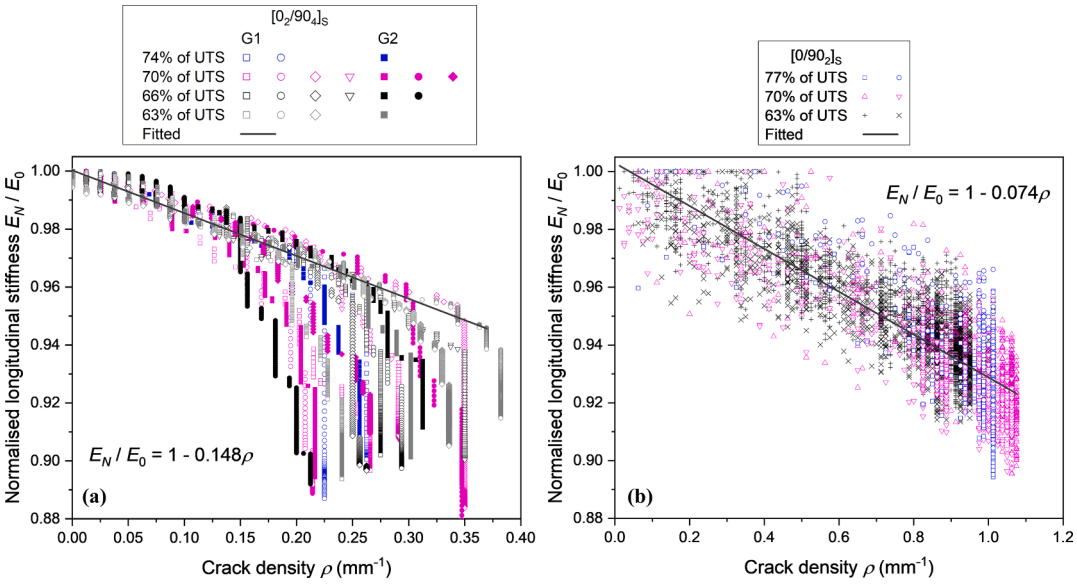

Fig. 14. Crack density versus normalised longitudinal stiffness for $[0_2/90_4]_s$ (a) and $[0/90_2]_s$ (b) laminates. (G1-Group 1; G2-Group 2).

For $[0_2/90_4]_s$ laminates, the similarity of the interaction between transverse cracks and delamination is also analysed with different stress levels involved. Fig. 15 shows the propagation of delamination along edges and inside specimens as crack density increases. Based on the saturated crack density ρ_s, specimens with $\rho_s = 0.21 \pm 0.01$, 0.26 ± 0.01, 0.3 ± 0.01 and 0.34 ± 0.01 mm^{-1} are classified into four groups for all stress levels. A faster increase of interlaminar crack ratio and normalised delamination area can be observed for specimens with lower saturated crack density, leading to larger delamination propagation along edges and inside specimens at the characteristic damage state. These phenomena indicate saturated crack density can reflect the severity of interaction between delamination and transverse cracks regardless of stress levels. The lower the saturated crack density is, the severer the interaction among both damage mechanisms exists for $[0_2/90_4]_s$ laminates.

Besides, the competitive relation between delamination propagation

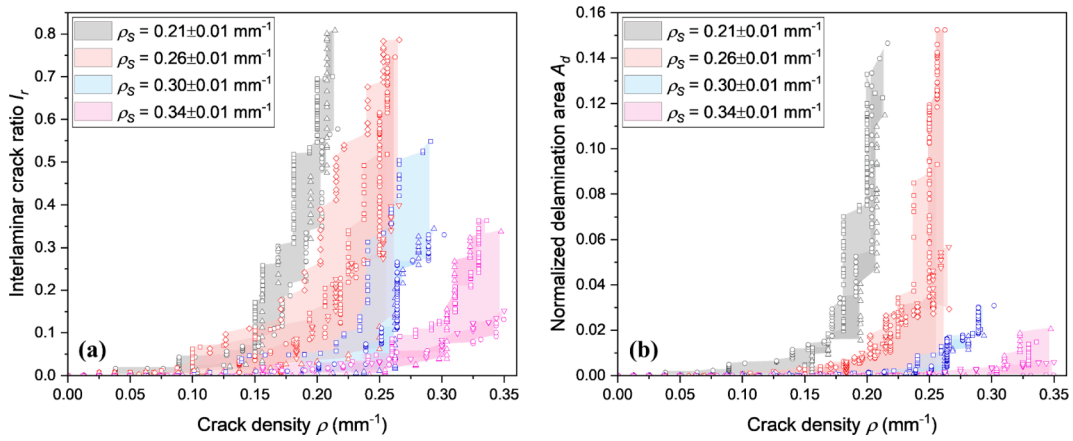

Fig. 15. The increase of interlaminar crack ratio (a) and normalised delamination ratio (b) with the increase of crack density for $[0_2/90_4]_s$ laminates. (ρ_s - saturated crack density).

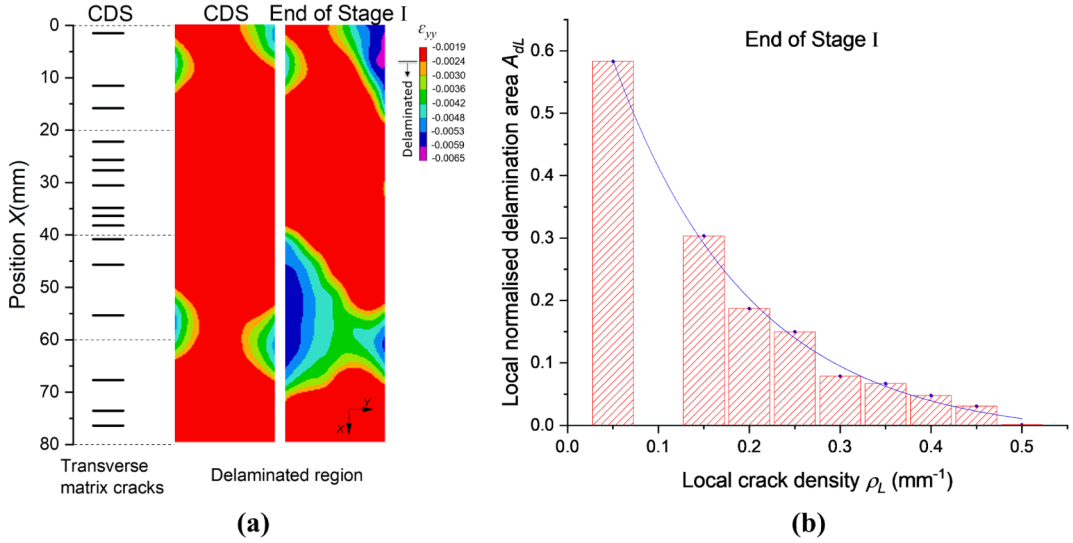

Fig. 16. Spatial distributions of transverse cracks and delamination at the characteristic CDS and end of Stage I of stiffness degradation for one of $[0_2/90_4]_s$ specimens tested under the stress level of 70% UTS (a); local normalised delamination area versus local crack density at the end of Stage I for $[0_2/90_4]_s$ laminates tested under all stress levels (b). (ε_{yy} - transverse strain).

and crack evolution is also presented in Fig. 15. To explore why the accumulation of these two damage mechanisms restrains each other, the spatial distribution of transverse cracks along edges, and the delamination within the gauge region are checked at the characteristic damage state and at the end of stage I of stiffness degradation. For an example, considering one of specimens tested under the stress level of 70% UTS, the position of transverse cracks is marked along the 80 mm gauge length, as shown in Fig. 16(a). In addition, the transverse strain concentration obtained from DIC is also presented, where the red means no delamination and the rest means delaminated region. As observed, delamination is prone to initiate and propagate at the local region with a large crack spacing. Further, the gauge region of specimens tested under all stress levels is evenly divided into four parts with 20 mm length. Then, the local crack density ρ_L and local normalised delamination area A_{dL} at the end of Stage I are quantified and summarised in Fig. 16(b), where A_{dL} is the mean value among all specimens. It is obvious that the relation between A_{dL} and ρ_L is nonlinear and the delaminated region is less than 10% when the local crack density is higher than 0.3 mm^{-1}.

5. Conclusions

Both the degradation of mechanical properties and accumulation of early fatigue damage for the $[0_2/90_4]_s$ and $[0/90_2]_s$ carbon/epoxy laminates were monitored and analysed under different stress levels. The main conclusions of the present study are summarised here.

1) For $[0_2/90_4]_s$ laminates, different levels of interaction between transverse cracks and delamination exist among specimens; the specimen with a lower saturated crack density presents severer interaction between both damage mechanisms. As for $[0/90_2]_s$ laminates, transverse cracks are the dominant damage mechanism.
2) An increase of Poisson's ratio during the early fatigue life is presented for $[0_2/90_4]_s$ laminates due to the growth of delamination, while $[0/90_2]_s$ laminates show the exact opposite trend caused by the accumulation of transverse cracks. This difference means that Poisson's ratio could be considered to identify whether the early fatigue damage is dominant by transverse cracks or involves delamination.

3) Cumulative AE energy is well correlated to crack density with the increase of fatigue cycles for both ply configurations, showing its potential as an indicator of crack density.
4) The effect of stress levels on the early fatigue damage accumulation is reflected on the growth rates of transverse cracks and delamination.

Declaration of Competing Interest

The authors declare that they have no known competing financial interests or personal relationships that could have appeared to influence the work reported in this paper.

Acknowledgements

The authors would like to thank the financial supports of China Scholarship Council (No.201706290028).

References

[1] Vassilopoulos AP. The history of fiber-reinforced polymer composite laminate fatigue. Int J Fatigue 2020;134:105512. https://doi.org/10.1016/j.ijfatigue.2020.105512.
[2] Samareh-mousavi SS, Mandegarian S, Taheri-behrooz F. A nonlinear FE analysis to model progressive fatigue damage of cross-ply laminates under pin-loaded conditions. Int J Fatigue 2019;119:290–301. https://doi.org/10.1016/j.ijfatigue.2018.10.010.
[3] Alderliesten RC, Brunner AJ, Pascoe JA. Cyclic fatigue fracture of composites: What has testing revealed about the physics of the processes so far? Eng Fract Mech 2018;203:186–96. https://doi.org/10.1016/j.engfracmech.2018.06.023.
[4] Huang J, Pastor ML, Garnier C, Gong XJ. A new model for fatigue life prediction based on infrared thermography and degradation process for CFRP composite laminates. Int J Fatigue 2019;120:87–95. https://doi.org/10.1016/j.ijfatigue.2018.11.002.
[5] Movahedi-Rad AV, Keller T, Vassilopoulos AP. Fatigue damage in angle-ply GFRP laminates under tension-tension fatigue. Int J Fatigue 2018;109:60–9. https://doi.org/10.1016/j.ijfatigue.2017.12.015.
[6] Li A, Huang J, Zhang C. Enabling rapid fatigue life prediction of short carbon fiber reinforced polyether-ether-ketone using a novel energy dissipation–based model. Compos Struct 2021;272:114227. https://doi.org/10.1016/j.compstruct.2021.114227.
[7] Maeck J, Abdel Wahab M, Peeters B, De Roeck G, De Visscher J, De Wilde WP, et al. Damage identification in reinforced concrete structures by dynamic stiffness determination. Eng Struct 2000;22(10):1339–49. https://doi.org/10.1016/S0141-0296(99)00074-7.
[8] Li X, Ma D, Liu H, Tan W, Gong X, Zhang C, et al. Assessment of failure criteria and damage evolution methods for composite laminates under low-velocity impact. Compos Struct 2019;207:727–39. https://doi.org/10.1016/j.compstruct.2018.09.093.
[9] Barbero EJ, Cortes DH. A mechanistic model for transverse damage initiation, evolution, and stiffness reduction in laminated composites. Compos B 2010;41(2):124–32. https://doi.org/10.1016/j.compositesb.2009.10.001.
[10] Ma D, González-Jiménez Á, Giglio M, dos Santos Cougo CM, Amico SC, Manes A. Multiscale modelling approach for simulating low velocity impact tests of aramid-epoxy composite with nanofillers. Eur J Mech A Solids 2021;90:104286. https://doi.org/10.1016/j.euromechsol.2021.104286.
[11] Reifsnider K, Jamison R. Fracture of fatigue-loaded composite laminates. Int J Fatigue 1982;4(4):187–97. https://doi.org/10.1016/0142-1123(82)90001-9.
[12] Pakdel H, Mohammadi B. Stiffness degradation of composite laminates due to matrix cracking and induced delamination during tension-tension fatigue. Eng Fract Mech 2019;216:106489. https://doi.org/10.1016/j.engfracmech.2019.106489.
[13] Shokrieh M-B, Taheri-Behrooz F. Progressive Fatigue Damage Modeling of Cross-ply Laminates, I: Modeling Strategy. J Compos Mater 2010;44:1217–31. https://doi.org/10.1177/0021998309351604.
[14] Taheri-Behrooz F, Shokrieh MM, Lessard LB. Progressive Fatigue Damage Modeling of Cross-ply Laminates, II: Experimental Evaluation. J Compos Mater 2010;44(10):1261–77. https://doi.org/10.1177/0021998309351605.
[15] Li X, Kupski J, Teixeira De Freitas S, Benedictus R, Zarouchas D. Unfolding the early fatigue damage process for CFRP cross-ply laminates. Int J Fatigue 2020;140:105820. https://doi.org/10.1016/j.ijfatigue.2020.105820.
[16] Li X, Kupski J, Teixeira De Freitas S, Benedictus R, Zarouchas D. Data underlying the article: Unfolding the early fatigue damage process for CFRP cross-ply laminates. 4TU ResearchData Dataset 2020. https://doi.org/10.4121/12927974.v1.
[17] Amacher R, Cugnoni J, Botsis J, Sorensen L, Smith W, Dransfeld C. Thin ply composites: Experimental characterization and modeling of size-effects. Compos Sci Technol 2014;101:121–32. https://doi.org/10.1016/j.compscitech.2014.06.027.
[18] Camanho PP, Dávila CG, Pinho ST, Iannucci L, Robinson P. Prediction of in situ strengths and matrix cracking in composites under transverse tension and in-plane shear. Compos A Appl Sci Manuf 2006;37(2):165–76. https://doi.org/10.1016/j.compositesa.2005.04.023.
[19] Kohler S, Cugnoni J, Amacher R, Botsis J. Transverse cracking in the bulk and at the free edge of thin-ply composites: Experiments and multiscale modelling. Compos A Appl Sci Manuf 2019;124:105468. https://doi.org/10.1016/j.compositesa:2019.05.036.
[20] Hosoi A, Kawada H. Fatigue life prediction for transverse crack initiation of CFRP cross-ply and quasi-isotropic laminates. Materials 2018;11(7):1182. https://doi.org/10.3390/ma11071182.
[21] Kötter B, Endres J, Körbelin J, Bittner F, Endres H-J, Fiedler B. Fatigue and fatigue after impact behaviour of Thin- and Thick-Ply composites observed by computed tomography. Composites Part C: Open Access 2021;5:100139. https://doi.org/10.1016/j.jcomc.2021.100139.
[22] Shen H, Yao W, Qi W, Zong J. Experimental investigation on damage evolution in cross-ply laminates subjected to quasi-static and fatigue loading. Compos B Eng 2017;120:10–26. https://doi.org/10.1016/j.compositesb.2017.02.033.
[23] Samareh-Mousavi SS, Taheri-Behrooz F. A novel creep-fatigue sti ff ness degradation model for composite materials. Compos Struct 2020;237:111955. https://doi.org/10.1016/j.compstruct.2020.111955.
[24] Hosoi A, Takamura K, Sato N, Kawada H. Quantitative evaluation of fatigue damage growth in CFRP laminates that changes due to applied stress level. Int J Fatigue 2011;33(6):781–7. https://doi.org/10.1016/j.ijfatigue.2010.12.017.
[25] Shabani P, Taheri-behrooz F, Samareh-mousavi SS, Shokrieh MM. Progress in Materials Science Very high cycle and gigacycle fatigue of fiber-reinforced composites : A review on experimental approaches and fatigue damage mechanisms. Prog Mater Sci 2021;118:100762. https://doi.org/10.1016/j.pmatsci.2020.100762.
[26] Hoang NT, Gamby D, Lafarie-Frenot M-C. Predicting fatigue transverse crack growth in cross-ply carbon-epoxy laminates from quasi static strength tests by using iso-damage curves. Int J Fatigue 2010;32(1):166–73. https://doi.org/10.1016/j.ijfatigue.2009.02.045.
[27] Saeedifar M, Zarouchas D. Damage characterization of laminated composites using acoustic emission: A review. Compos B Eng 2020;195:108039. https://doi.org/10.1016/j.compositesb:2020.108039.
[28] Hexcel. HexPly ® 6376 - Product Data Sheet - EU Version 2016:1–2.
[29] ASTM International. D3479/D3479M-19 Standard Test Method for Tension-Tension Fatigue of Polymer Matrix Composite Materials. West Conshohocken, PA; ASTM International 2019. https://doi.org/10.1520/D3479_D3479M-19.
[30] Berthelot J-M, Mahi AE, Le Corre J-F. Development of transverse cracking in cross-ply laminates during fatigue tests. Compos Sci Technol 2001;61(12):1711–21. https://doi.org/10.1016/S0266-3538(01)00068-9.
[31] Li X, Saeedifar M, Benedictus R, Zarouchas D. Damage accumulation analysis of cfrp cross-ply laminates under different tensile loading rates. Composites Part C: Open Access 2020;1. https://doi.org/10.1016/j.jcomc.2020.100005.
[32] Oz FE, Ersoy N, Mehdikhani M, Lomov SV. Multi-instrument in-situ damage monitoring in quasi-isotropic CFRP laminates under tension. Compos Struct 2018;196:163–80. https://doi.org/10.1016/j.compstruct.2018.05.006.
[33] Pakdel H, Mohammadi B. Characteristic damage state of symmetric laminates subject to uniaxial monotonic-fatigue loading. Eng Fract Mech 2018;199:86–100. https://doi.org/10.1016/j.engfracmech.2018.05.007.
[34] Carraro PA, Maragoni L, Quaresimin M. Characterisation and analysis of transverse crack-induced delamination in cross-ply composite laminates under fatigue loadings. Int J Fatigue 2019;129:105217. https://doi.org/10.1016/j.ijfatigue.2019.105217.
[35] Pakdel H, Mohammadi B, Hosseini-Toudeshky H. Stress and energy based prediction of crack distribution pattern in general cross-ply laminates. Eng Fract Mech 2020;223:106769. https://doi.org/10.1016/j.engfracmech.2019.106769.
[36] Naderi M, Kahirdeh A, Khonsari MM. Dissipated thermal energy and damage evolution of Glass/Epoxy using infrared thermography and acoustic emission. Compos B Eng 2012;43:1613–20. https://doi.org/10.1016/j.compositesb.2011.08.002.
[37] Zhang Z, Yang G, Hu K. Prediction of fatigue crack growth in gas turbine engine blades using acoustic emission. Sensors (Switzerland) 2018;18. https://doi.org/10.3390/s18051321.
[38] Chen C, Chen X, Guo S. Experimental study on acoustic emission characteristic of fatigue crack growth of self-compacting concrete. Structural Control and Health Monitoring 2019;26:1–17. https://doi.org/10.1002/stc.2332.
[39] Baker C, Morscher GN, Pujar VV, Lemanski JR. Transverse cracking in carbon fiber reinforced polymer composites: Modal acoustic emission and peak frequency analysis. Compos Sci Technol 2015;116:26–32. https://doi.org/10.1016/j.compscitech.2015.05.005.
[40] Silberschmidt VV. Matrix cracking in cross-ply laminates: Effect of randomness. Compos A Appl Sci Manuf 2005;36:129–35. https://doi.org/10.1016/j.compositesa.2004.06.008.
[41] Glud JA, Dulieu-barton JM, Thomsen OT, Overgaard LCT. Fatigue damage evolution in GFRP laminates with constrained off-axis plies. Compos A 2017;95:359–69. https://doi.org/10.1016/j.compositesa.2017.02.005.
[42] Montesano J, McCleave B, Singh CV. Prediction of ply crack evolution and stiffness degradation in multidirectional symmetric laminates under multiaxial stress states. Compos B Eng 2018;133:53–67. https://doi.org/10.1016/j.compositesb.2017.09.016.